

Small-scale filament eruptions as the driver of solar coronal hole X-ray jets

Alphonse C. Sterling¹, Ronald L. Moore^{2,1}, David A. Falconer^{2,1}, & Mitzi Adams¹

¹NASA/Marshall Space Flight Center, Huntsville, Alabama 35812

²Center for Space Plasma and Aeronomic Research, University of Alabama in Huntsville, Huntsville, AL 35899

Solar X-ray jets are evidently made by a burst of reconnection of closed magnetic field in a jet's base with ambient "open" field^{1,2}. In the widely-accepted version of the "emerging-flux" model, that reconnection occurs at a current sheet between the open field and emerging closed field and also makes a compact hot brightening that is usually observed at the edge of the jet's base^{1,3}. Here we report on high-resolution X-ray and EUV observations of 20 randomly-selected X-ray jets in polar coronal holes. In each jet, contrary to the emerging-flux model, a miniature version of the filament eruptions that initiate coronal mass ejections (CMEs)⁴⁻⁷ drives the jet-producing reconnection, and the compact hot brightening is made by internal reconnection of the legs of the minifilament-carrying erupting closed field, analogous to solar flares of larger-scale eruptions. Previous observations have found that some jets are driven by base-field eruptions^{8-10,12}, but only one such study, of only one jet, provisionally questioned the emerging-flux model¹³. Our observations support the view that solar filament eruptions are made by a fundamental explosive magnetic process that occurs on a vast range of scales, from the biggest CME/flare eruptions down to X-ray jets, and perhaps down to

even smaller jets that are candidates for powering coronal heating^{10,14,15}. A picture similar to that suggested by our observations was drawn before, inferred from different observations and based on a different origin of the erupting minifilament flux rope¹¹ (see Methods).

Solar X-Ray jets are imaged from space in the ~ 0.2 — 2.0 keV range. They are dynamic (upward velocities ~ 200 km s⁻¹), long ($\sim 5 \times 10^4$ km), narrow (8×10^3 km), and transient (lifetimes ~ 10 min)^{16,17}. In the commonly-accepted version of the emerging-flux model^{3,18-21}, an emerging bipole enters a dominant-polarity (say, negative) ambient open field, and the bipole’s minority-polarity (positive) side can reconnect with coronal field at the location of the magnetic null region between the bipole and the ambient field. In this model, a burst of reconnection connects the outside of the bipole with adjacent coronal field, producing a small loop on the outside of the emerging bipole’s minority-polarity foot, and reconnects open field to the outside of the bipole’s majority-polarity foot. An X-ray jet develops as reconnection-heated material flows out along the new open field strands. Additionally, the reconnection-formed small loop at the emerging field’s edge is the model’s explanation for the observed base-edge compact X-ray jet bright point (JBP). In a later-suggested extension of the emerging-flux model, the emerged bipole explodes as it reconnects, forming a “blowout jet” with a relatively-broad spire¹⁵. (See Methods and Extended Data Fig. 1 for details of the emerging-flux model.)

To assess observationally the production of X-ray jets, we analysed 20 jets (Extended Data Table 1) in the solar polar regions using X-ray images from the X-ray telescope (XRT) on the *Hinode* satellite²², which detects a broad temperature range of coronal plasmas hotter than about

1.5 MK. We used concurrent EUV images from the Solar Dynamics Observatory’s (*SDO*) Atmospheric and Imaging Assembly (AIA)²³, whose various filters detect plasmas primarily over narrow temperature ranges centred at, e.g. $T \approx 0.05, 0.6, 1.6,$ or 2.0 MK respectively for wavelengths of $304 \text{ \AA}, 171 \text{ \AA}, 193 \text{ \AA}, 211 \text{ \AA}$. (See Methods.)

Figure 1 shows a typical example of our results in both soft X-ray (Figs. 1a—1c) and EUV (Figs. 1d—1f) images. Between Figures 1a and 1b the jet’s spire, arched base, and JBP all begin brightening. Later (Fig. 1c) the spire extends higher, with the JBP positioned about $10''$ west of the spire. From a movie constructed from the XRT images (see Extended Data Video 1abc), the JBP brightening starts at $\sim 22:07$ UT, with the spire becoming visible ~ 2.5 min later. Thus one can imagine this jet obeyed the emerging-flux model, where *external reconnection* (i.e., reconnection occurring on the outside of the closed driving field²⁴) of emerging field forms the JBP and gives rise to the spire at a displaced location. Observing the same feature in AIA 193 \AA EUV images (Fig. 1, and in Extended Data Video 1def) however does *not* support this interpretation. These images clearly show a dark feature, similar to a small-scale solar chromospheric filament (hereafter, “minifilament”), moving upward and laterally, starting from $\sim 22:06$ UT. Its velocity is $\sim 40 \text{ km s}^{-1}$ between $22:07$ UT and $\sim 22:10$ UT, when it reaches the apex of the illuminated arched base of the X-ray jet. After $22:10$ UT, the minifilament is expelled in the spire of an EUV jet that is the counterpart to the XRT jet. In EUV the jet has both emission and absorption components, with the minifilament evolving into part of the jet. Significantly however, the JBP, both in soft X-rays and in EUV, is at the location from where the minifilament erupted. Thus the JBP is the analog to the commonly-observed solar flare arcade forming in the wake of larger-scale filament

eruptions; such flare arcades are made by *internal reconnection* (i.e., reconnection occurring on the inside of the closed driving field²⁴) of the legs of the erupting closed field of a filament. This is *not* consistent with the JBP resulting from external reconnection as proposed in the emerging-flux model.

We found an erupting minifilament to be discernible in AIA images of all 20 of the jets, with the minifilament's eruption starting near the location of the JBP. In most cases we could see that the JBP occurred where the minifilament (or part of the minifilament) had been rooted in the surface prior to ejection; we could not verify this arrangement in a few cases where the minifilament and JBP were along the same line-of-sight, but even then the observations are consistent with the JBP occurring at the location from where the minifilament was ejected. Typically, first the minifilament starts to lift off from the surface, and then the JBP starts to brighten. This is similar to the situation with large-scale filament eruptions, where the eruption start precedes the flare-brightening onset²⁵. Other than size scale, the eruptions of minifilaments in the production of X-ray jets are indistinguishable from the commonly-observed eruptions of larger filaments in the onsets of solar flares. In some cases (in Extended Data Table 1, events 4, 9 and 13, and maybe event 1), rather than the entire minifilament lifting off, there is a whipping-like motion, with the JBP (flare) occurring below the whipping minifilament or at the location where the fastest-moving part of the minifilament first detaches from the solar surface. Thus all cases are consistent with the JBP being a small flare arcade forming in the wake of the erupting minifilament⁴⁻⁷.

We measured the plane-of-sky sizes and velocities of the minifilaments, during the period

after they started to erupt but prior to reaching the jet-spire location. The average length of the minifilaments were $11''$ ($= 8 \times 10^3$ km) with a standard deviation of $4''$. This is much smaller than the sizes quoted for filaments from an extensive survey²⁶ (3×10^4 — 1.1×10^5 km), justifying the term “minifilaments”. (Perhaps-identical minifilaments have been identified on the solar disk²⁷.) Our measured average minifilament size is equal to the average width of X-ray jets¹⁷, consistent with the jets being driven by the minifilament eruptions. We obtained mean velocities and a standard deviation for the erupting minifilaments of 31 ± 15 km s⁻¹. In all cases the true sizes and speeds should tend to be larger than these plane-of-sky values.

X-ray jets have been classified as “standard” or “blowout” based on the morphology of the spire and the intensity of the rest of the jet’s base compared to the JBP intensity: A standard jet has a narrow spire with a relatively dim base, while a blowout jet has a broad spire and a base that becomes about as bright as the JBP¹⁵. The emerging-flux model suggests that the difference occurs depending on whether the emerging-flux structure remains largely inert (standard jet), or erupts (blowout jet) as the jet forms. Our new view is different: In a previous study¹⁵ of our 20 events, we morphologically classified 14 as blowout, five as standard, and one as ambiguous. We now find however that all 20 appear to form the same way: from erupting filaments. A jet has blowout-jet morphology if the erupting filament strongly ejects from the base region (corresponding to an ejective larger-scale solar eruption⁶). Standard-jet morphology seems to result when the erupting minifilament mainly does not escape the closed-field base (maybe corresponding to confined larger-scale filament eruptions⁶), or perhaps if the eruption is ejective but very weak. We envision that there is a continuum of morphological jet types, likely depending on the eruption’s

strength and whether the erupting filament escapes the base.

From our observations we infer the schematic picture of Figure 2 for jet production. Initially (Fig. 2a) two bipoles sit side-by-side, the larger one corresponding to what we usually observe as the base of the jet (cf. Fig. 1). The smaller bipole contains substantial free energy in sheared and twisted magnetic field; that field holds a minifilament. As with the case of large-scale solar eruptions, this field becomes unstable by some process; it then erupts outward, guided between the large bipole and the ambient open field. After the minifilament's liftoff, reconnection occurs among the distended legs of the minifilament field (Fig. 1b), making a "flare-arcade" JBP via internal reconnection occurring inside the erupting field. The spire starts as soon as the outer envelope of the minifilament-carrying erupting field starts external reconnection with open field on the far side of the large bipole. External reconnection continues and soon reconnects the field threading the erupting minifilament with far-side open field, injecting minifilament plasma along that open field. The external reconnection also adds a new hot layer to the larger bipole (larger red loop in Fig. 2c).

If the erupting minifilament-carrying field blows out beyond the large bipole's apex (Figs 2b—2c), then widespread external reconnection results; this creates a broad jet spire characteristic of blowout jets. If the erupting field stalls near the apex of the large bipole (and/or if the eruption is weak enough), the external reconnection produces only a narrow jet, characteristic of a standard jet. Examples of blowout jets are in Figure 1, and in Extended Data Figures 2 and 3 and their corresponding videos (Extended Data Videos 2abc, 2def, 3abc and 3def). Examples of standard jets

are in Extended Data Figures 4 and 5 and their corresponding videos (Extended Data Videos 4abc, 4def, 5abc and 5def).

The flux-emergence model fails to explain the observation of a JBP occurring below the erupting minifilament, which the Figure 2 picture naturally explains. Also, an expectation of the emerging-flux model is that, as the external reconnection progresses, reconnected open field will stand progressively closer to the JBP than that from earlier reconnection¹⁹. That is, the jet spire should drift *toward* the JBP with time in that model. Observations however show that more often than not the spire drifts *away* from the JBP with time²⁸. The schematic of Figure 2 naturally explains this proclivity for spire drift away from the JBP, since the external reconnection of the erupting minifilament-carrying field produces reconnected open field lines that in the corona stand progressively further away from the eruption's source location, which is the location of the internal-reconnection flare arcade that is the JBP.

We have not addressed what leads to our minifilament eruptions. Some recent studies of on-disk coronal jets found the miniature filaments to have likely resulted from cancelation of magnetic flux in the hours leading up to the eruption^{13,29,30}. We suspect that, as with large-scale eruptions, various agents could trigger the eruption, including flux cancellation and flux emergence. For triggering by flux emergence, the emergence would *trigger the minifilament's eruption*, rather than directly drive the jet as proposed in the emerging-flux model for jets.

The minority-polarity flux in the base of the an X-ray jet presumably comes from flux emergence of compact field loops into the dominant-polarity ambient field. It therefore seems that

many X-ray jets should be produced by these closed-field emergences in the manner of the long-accepted emerging-flux model. Our observation of no such X-ray jets (at least for polar coronal holes) suggests that external reconnection of the emerging closed field with the ambient open field continually occurs fast enough to keep an appreciable current sheet from building up at the magnetic null between the two fields, and a burst of enough external reconnection to make an X-ray jet can be made only dynamically, driven by sudden eruption of the closed field as in a filament eruption. That is, the observed lack of emerging-flux-model X-ray jets suggests that no current sheet of the scale of the overall system of two reconnecting fields can be formed gradually (i.e., quasi-stably) in the low-beta magnetised plasma of X-ray jets, and by analogy nor in similar reconnection events in other low-beta astrophysical settings.

1. Shibata, K. *et al.* Observations of x-ray jets with the yohkoh soft x-ray telescope. *Pub. Astro. Soc. Japan* **44**, 173L–179L (1992).
2. Cirtain, J. W. *et al.* Evidence for alfvén waves in solar jets. *Science* **318**, 1580–1582 (2007).
3. Yokoyama, T. & Shibata, K. Magnetic reconnection as the origin of x-ray jets and H α surges on the sun. *Nature* **375**, 42–44 (1995).
4. Hirayama, T. Theoretical model of flares and prominences. *Solar Phys.* **34**, 323–338 (1974).
5. Shibata, K. *et al.* Hot-plasma ejections associated with compact-loop solar flares. *Astrophys. J.* **451**, L83–L85 (1995).

6. Moore, R. L., Sterling, A. C., Hudson, H. S. & Lemen, J. R. Onset of the magnetic explosion in solar flares and coronal mass ejections. *Astrophys. J.* **552**, 833–848 (2001).
7. Chen, P. F. Coronal mass ejections: models and their observational basis. *Solar Phys.* **8**, 1 (2011).
8. Moore, R. L., Tang, F., Bohlin, J. D. & Golub, L. H-alpha macrospicules - identification with euv macrospicules and with flares in x-ray bright points. *Astrophys. J.* **218**, 286–290 (1977).
9. Sterling, A. C., Harra, L. K. & Moore, R. Fibrillar chromospheric spicule-like counterparts to an extreme-ultraviolet and soft x-ray blowout coronal jet. *Astrophys. J.* **722**, 1644–1653 (2010).
10. Raouafi, N.-E., Georgoulis, M. K., Rust, D. M. & Bernasconi, P. N. Micro-sigmoids as progenitors of coronal jets: is eruptive activity self-similarly multi-scaled? *Astrophys. J.* **718**, 981–987 (2010).
11. Shibata, K. Evidence of Magnetic Reconnection in Solar Flares and a Unified Model of Flares *Astrophys. and Sp. Sci.* **264**, 129–144 (1999).
12. Nisticò, G., Bothmer, V., Patsourakos, S. & Zimbardo, G. Characteristics of euv coronal jets observed with stereo/secchi. *Solar Phys.* **259**, 87–108 (2009).
13. Adams, M., Sterling, A. C., Moore, R. L. & Gary, G. A. A small-scale eruption leading to a blowout macrospicule jet in an on-disk coronal hole. *Astrophys. J.* **783**, 11–24 (2014).
14. De Pontieu, B. *et al.* The origins of hot plasma in the solar corona. *Science* **331**, 55–58 (2011).

15. Moore, R. L., Sterling, A. C., Falconer, D. A. & Robe, D. The cool component and the dichotomy, lateral expansion, and axial rotation of solar x-ray jets. *Astrophys. J.* **769**, 134–153 (2013).
16. Shimojo, M. *et al.* Statistical study of solar x-ray jets observed with the yohkoh soft x-ray telescope. *Pub. Astro. Soc. Japan* **48**, 123–136 (1996).
17. Savcheva, A. *et al.* A study of polar jet parameters based on Hinode XRT observations. *Pub. Astro. Soc. Japan* **59**, S771–S778 (2007).
18. Nishizuka, N. *et al.* Giant chromospheric anemone jet observed with Hinode and comparison with magnetohydrodynamic simulations: evidence of propagating alfvén waves and magnetic reconnection. *Astrophys. J.* **683**, L83–L86 (2008).
19. Moreno-Insertis, F. & Galsgaard, K. Plasma jets and eruptions in solar coronal holes: a three-dimensional flux emergence experiment. *Astrophys. J.* **771**, 20–38 (2013).
20. Archontis, V. & Hood, A. W. A numerical model of standard to blowout jets. *Astrophysical. J.* **769**, L21–L26 (2013).
21. Fang, F., Fan, Y. & McIntosh, S. W. Rotating solar jets in simulations of flux emergence with thermal conduction. *Astrophys. J.* **789**, L19–L25 (2014).
22. Kosugi, T. *et al.* The Hinode (solar-b) mission: an overview. *Solar Phys.* **243**, 3–17 (2007).
23. Lemen, J. R. *et al.* The atmospheric imaging assembly (AIA) on the solar dynamics observatory (SDO). *Solar Phys.* **275**, 17–40 (2012).

24. Sterling, A. C. & Moore, R. L. Internal and external reconnection in a series of homologous solar flares. *J. Geophys. Res.* **106**, 25227–25238 (2001).
25. Sterling, A. C. & Moore, R. L. Slow-rise and fast-rise phases of an erupting solar filament, and flare emission onset. *Astrophys. J.* **630**, 1148–1159 (2005).
26. Bernasconi, P. N. & Rust, D., D. M. & Hakim. Advanced automated solar filament detection and characterization code: description, performance, and results. *Solar Phys.* **228**, 971–117 (2005).
27. Wang, J. *et al.* Minifilament eruption on the quiet sun. I. observations at H α central line. *Astrophys. J.* **530**, 1071–1084 (2000).
28. Savcheva, A., Cirtain, J. W., DeLuca, E. E. & Golub, L. Does a polar coronal hole's flux emergence follow a hale-like law? *Astrophys. J.* **702**, L32–L36 (2009).
29. Shen, Y., Liu, Y., Su, J. & Deng, Y. On a coronal blowout jet: the first observation of a simultaneously produced bubble-like CME and a jet-like CME in a solar event. *Astrophys. J.* **745**, 164–172 (2012).
30. Young, P. R. & Muglach, K. A. Solar dynamics observatory and Hinode observations of a blowout jet in a coronal hole. *Solar Phys.* **289**, 3313–3329 (2014).

Acknowledgements A.C.S. and R.L.M. were supported by funding from the Heliophysics Division of NASA's Science Mission Directorate through the Living With a Star Targeted Research and Technology Program (LWS TR&T), and the Hinode Project. Both benefited from TR&T discussions and from discussions with S. K. Antiochos. ACS also benefited from discussions held at the International Space Science Institute's (ISSI; Bern, Switzerland) International Team on Solar Coronal Jets (Team Lead: N. Raouafi).

Author Contributions A.C.S.: Reduction, analysis, and interpretation of XRT and AIA data; software development; manuscript preparation. R.L.M.: Interpretation of results, manuscript review. D.A.F.: Software development, assimilation and calibration of AIA data. M.A.: Discovery and analysis of seminal jet event motivating this broader investigation, manuscript review.

Author Information The authors declare that they have no competing financial interests. Correspondence and requests for materials should be addressed to A.C.S. (email: alphonse.sterling@nasa.gov) or R.L.M. (ron.moore@nasa.gov).

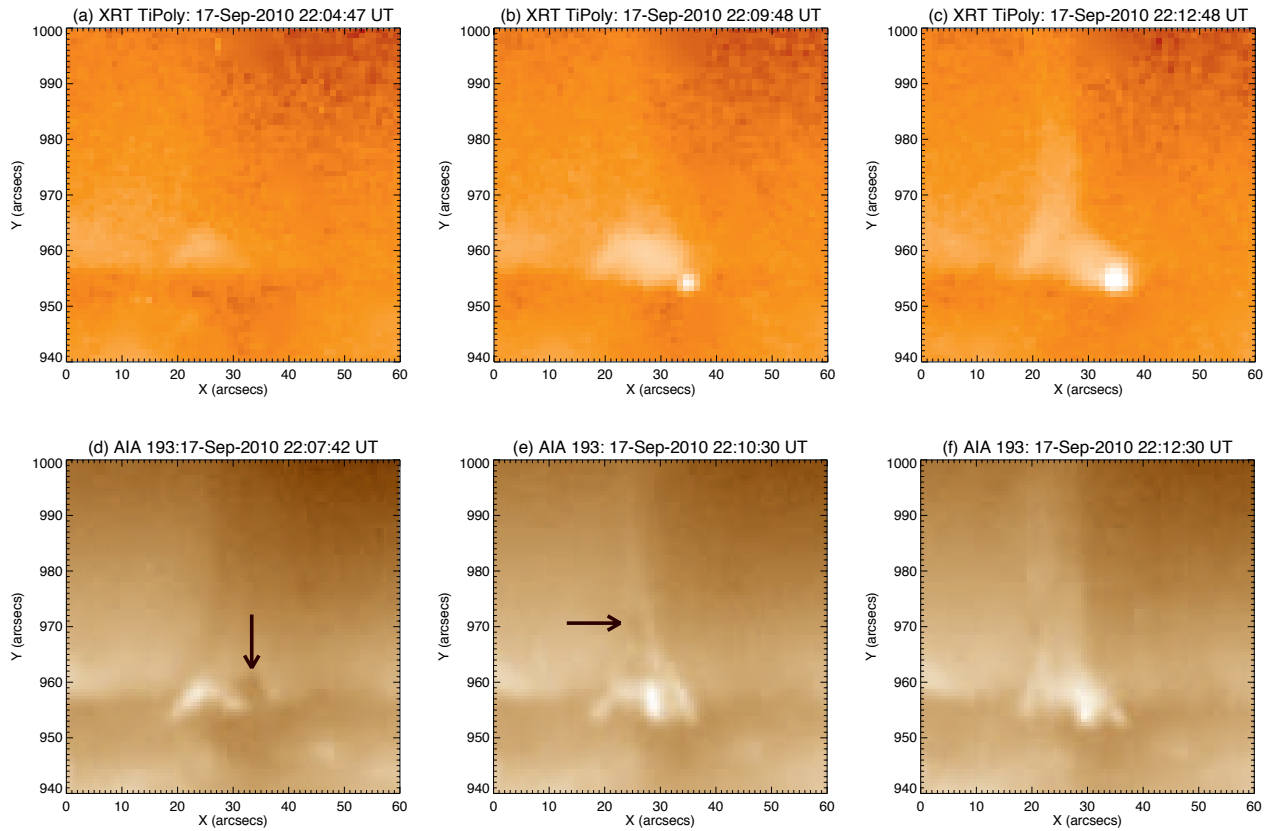


Figure 1. Erupting-Jet Example. Jet in soft X-rays (*Hinode*/XRT; a—c) and EUV (*SDO*/AIA 193 Å; d—f). The jet bright point (JBP) is visible by the time of (b), and the jet is fully developed and offset eastward of the JBP in (c). Arrows show a minifilament moving outward from the JBP location. North is upward and west is to the right. Panels a and d, b and e, and c and f are 217s, 30s, and 6s apart, respectively. See Methods for details, and Extended Data for animations (Extended Data Video 1abc and 1def). This is event 18 of Extended Data Table 1.

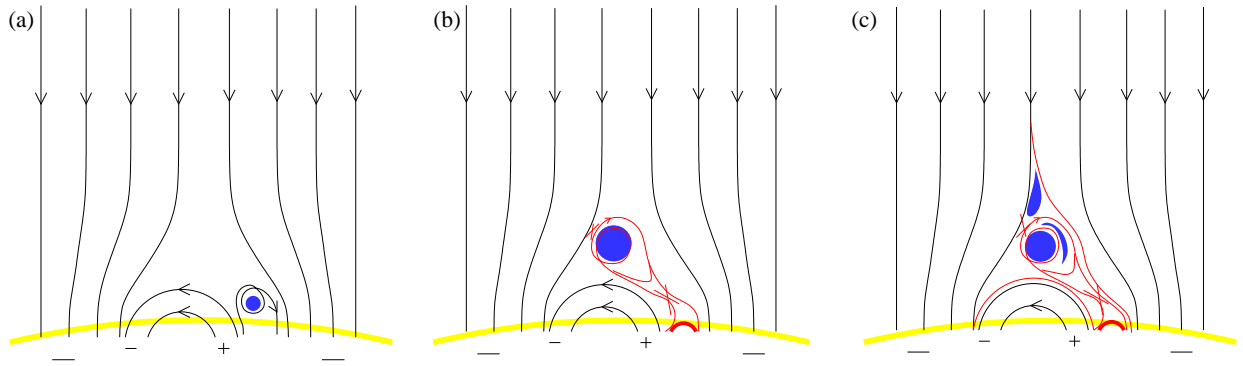


Figure 2. Revised Jet-Eruption Picture. Schematic representation of the minifilament-eruption process that drives X-ray jets, as inferred from our observations. Black lines represent magnetic field, with arrows indicating polarities; red curves are newly-reconnected field lines, blue features are minifilament material, and yellow curve is the solar limb. From the initial state (a), the jet forms as the minifilament erupts (b and c), with reconnection locations indicated by red X-es (b and c). The JBP (bold red arc) forms at the location of filament liftoff (b and c). See Methods for more details.

Methods

Emerging-flux model. According to the emerging-flux model^{2,3,18–20} (Extended Data Fig. 1) for solar coronal jets, an emerging bipole enters a dominant-polarity (negative in Extended Data Fig. 1) ambient open field, and the bipole’s minority-polarity (positive) side can reconnect with coronal field at the location of the magnetic null region between the bipole and the ambient field. After enough emergence of the bipole, a burst of reconnection joins the outside of the bipole with nearby coronal field (Extended Data Fig. 1b), resulting in two reconnection products: a small loop on the outside of the base of the emerging bipole’s minority-polarity side, and an open field connecting the bipole’s majority-polarity side with open coronal field, giving a new footpoint connection for that coronal field. This type of reconnection has been called “interchange”³¹, or “external”²⁴, since the reconnection is on the outside of the closed driving field (the emerging field in this case). An X-ray jet develops as reconnection-heated material flows out along the new open field strands. Additionally, the external-reconnection-formed small loop at the emerging field’s edge is the model’s explanation for the observed base-edge compact X-ray jet bright point (JBP; also called a “hot loop”³). In the previous view of blowout jets, the idea was that the external reconnection causes and/or is driven by ejective eruption (blowout) of the emerging bipole, which is assumed to contain substantial non-potential (i.e. twisted) magnetic field, driving that bipole’s eruption along the ambient open field to make a broad jet spire¹⁵.

Instrumentation and data. For our X-ray images, we use data from the *Hinode*/XRT with 30 s cadence and 1'' pixels. XRT detects a broad range of temperatures, but has highest sensitivity for temperature $T \gtrsim 1.5$ MK, even for the relatively cool “TiPoly”-filter images that we used for these

observations. For each jet in Extended Data Table 1 we studied concurrent EUV images from the SDO/AIA, with $0''.6$ pixels and 12 s cadence. Our final movies and figures were formed by summing the frames in pairs, and therefore the resulting movies we used were generally of 1-min cadence and 24-sec cadence respectively for XRT and AIA. This summing blurs the images somewhat, but renders subtle features, such as X-ray jets and some of the fainter EUV minifilaments, much easier to discern. For many of the X-ray jets of our study, we examined all the AIA EUV channels, which are tuned to wavelengths of 304 Å, 171 Å, 193 Å, 211 Å, 131 Å, 335 Å, and 94 Å; these respectively have strong responses to log temperatures (K) of: $\approx 4.7, 5.8, 6.2, 6.3, 7.0, 6.4,$ and 6.8 (although some channels are multivalued²³). Usually there was little new information in the hotter 131 Å, 335 Å, and 94 Å channels, and so we did not inspect these hotter channels for some of the jets.

In total we examined 20 X-ray jets, initially selected during an earlier study¹⁵, where the JBP was obvious in the X-ray images (Extended Data Table 1). From the previous study¹⁵, each event of Extended Data Table 1 is typed as “standard”, “blowout”, or “ambiguous”, based on its morphology in the XRT images (and in some cases, in AIA 304 Å images also). Blowout jets are those where the entire base brightened and where the spire broadened with time to span approximately the width of the base, while standard jets are those where only the JBP brightened substantially in the base and the spire remained narrow compared to the span of the base. The JBP is also referred to by other terms, including “hot loop”³, “bright loop”³, “bright point”^{3, 15, 32}, and “bright footpoint”¹⁷.

In each blowout jet in Extended Data Table 1 the minifilament eruption was evidently ejec-

tive; the erupting closed field apparently blows out into the ambient open field. In this case, much or all of the filament material escapes from the closed field onto the open field.

In the events of Extended Data Table 1 categorised as standard jets, a minifilament eruption was detectable, but usually that eruption appeared either not be ejective, or it was perhaps ejective but weak and/or faint. In event 4, a minifilament (best seen in 304 Å) has a whipping motion from the location that becomes the JBP. Event 7 seems to be generated by a minifilament that becomes partially destabilized and spins (rolls) beneath confining magnetic fields. These standard-jet events therefore may be analogous to larger-scale confined filament eruptions, ones that make flares that are of shorter duration than the ejective flares⁶. (As an example, the rolling minifilament of Event 7 could be a scaled-down version of the confined filament eruption in Fig. 1 and in the corresponding on-line movies of the paper Sterling *et al.* 2011³⁶.) Event 6, another standard jet, however shows an ejective minifilament, similar to the jets identified as blowout jets, but it does not make a broad spire. In that case it appears as if the minifilament erupted far enough for much of it to escape onto open field via external reconnection, but not enough to blow out violently and make a broad jet. In comparison to the blowout jets, more of the filament material remains trapped within the closed field.

Our other standard jets (5, 19), and the ambiguous jet (11), similarly may be partially-confined and partially-ejective minifilament eruptions. In these cases, some of the minifilament material escapes onto the open field, and some of it remains in the closed field. In this sense, we envision a continuum of jets manifestations, between pure blowout jet (where the filament field would push far into the opposite-polarity open field, making a broad jet, and all of the fila-

ment material would eventually escape onto that open field), and a pure standard jet (where only the envelope of the closed filament field reconnects with the opposite-polarity open field, and none of closed field containing the cool filament material undergoes external reconnection). Our view of standard jets being due to confined minifilament eruptions, partially-confined minifilament eruptions, and/or weak ejective minifilament eruptions, is still speculative. Further study will be required to understand fully various morphological differences among jets.

Minifilament measurement details. We measured the line-of-sight lengths and velocities of the minifilaments during the period after they started to erupt but prior to when they formed a jet or reached the apex of the base (below the jet spire). We usually used the 171 Å, 193 Å, or 211 Å AIA channels for these measurements; only for events 4, 7 and 10 did we find 304 Å preferable for determining minifilament properties in our data set. We obtained mean velocities for the erupting minifilaments of $31 \pm 15 \text{ km s}^{-1}$; if the velocities are weighted inversely with their uncertainty (Extended Data Table 1), the weighted mean velocity and weighted standard deviation are 24 km s^{-1} and 13 km s^{-1} , respectively.

Details of jet-formation process in our picture. As shown in Fig. 2, we envision that initially a minifilament-carrying, non-potential, relatively-compact core field of a magnetic bipole (or magnetic arcade) sits next to (and shares the minority-polarity flux with) a relatively-large bipole (Fig. 2a). An unspecified process destabilizes the smaller bipole so that it erupts, with the minifilament being channeled between the large bipole and the overlying open field. Upon reaching the open coronal field on the far side of the large bipole, the field carrying the minifilament reconnects with that field (Fig. 2b), and a jet, often including substantial minifilament material, is ejected

along newly-reconnected open field (Fig. 2c). This reconnection also adds field to the large bipole. Also in (Fig. 2b), internal reconnection (lower red X) of the minifilament-carrying field occurs; this is reconnection internal to the erupting lobe of the double bipole, and this reconnection forms a flare arcade (the JBP) in the wake of the ejected minifilament.

This is analogous to the formation of commonly-observed flare arcades in typical large-scale solar eruptions; that is, the erupting lobe of the system erupts as in a “typical” large-scale eruption, as pictured in, e.g., Figure 1 of Shibata *et al.* (1995)⁵ or Figure 1 of Moore *et al.* (2001)⁶. In our jet-formation picture, this process is occurring on a smaller scale so that the filament of those typical models corresponds to our minifilaments. Rather than a filament traveling directly outward as in those schematics of large-scale eruptions, in the jet case of Figure 2 the minifilament travels along the curved path between the adjacent bipole and distorted ambient coronal field. (The coronal field is distorted by the magnetic field of the two bipoles.) As long as the erupting minifilament is on the near-side (i.e., the side of its origin) of the apex of the neighboring bipole, no reconnection occurs between the erupting-bipole field enveloping the filament and ambient coronal fields. (In 3D the situation will not be as pure as in the 2D schematic, but we still expect the basic situation of the 2D schematic to hold.) We will consider what happens when the enveloping field reaches the far side of the apex shortly. First however, again looking at the schematics of the typical large-scale eruptions, it can be seen that the field lines beneath the erupting filament reconnect (this is what we are calling internal reconnection, since it occurs internal to the erupting bipole) to form hot flare loops near the solar surface. In our analogous schematic for the jets in Figure 2, these flare loops correspond to the JBP. While the small lobe of the double bipole in Fig. 2 is erupting in this

fashion, the neighboring bipole largely remains inert, except for the addition of the new field via the external reconnection, as mentioned in the previous paragraph.

Now consider the situation when the erupting-minifilament bipole reaches the far side of the apex of the neighboring bipole (Fig. 2b). Because the field orientations are then opposite, the erupting field enveloping the minifilament and the far-side ambient coronal field can undergo reconnection; since this reconnection is between the field of the erupting bipole and coronal field that is external to that erupting bipole, we call this external reconnection. This external reconnection adds heat to the reconnected field lines, making a hot jet spire along the open field lines and making hot loops over the adjacent bipole (red curves in Fig. 2c). This external reconnection progressively erodes away the field enveloping the cool minifilament material. If this erosion of that enveloping field stops before the field lines holding cool material is reached—which could happen, for example, if the erupting minifilament-carrying bipole does not have enough energy to travel deep into the far-side ambient-field region—then the cool material never makes it onto the open field (and the spire receives no cool material). Rather, the filament plasma remains trapped in closed field in the base of the jet. This may be how the standard jets are formed; only a narrow hot spire forms if the erupting minifilament-carrying bipole does not go far into the ambient-field region.

In a blowout jet, the eruption continues deeper into the opposite-directed ambient field region to make a broader spire than is depicted in Fig. 2c. The envelope around the cool-minifilament material is completely eroded away, and so the cool material escapes onto the open ambient coronal field, forming a cool jet. In this sense, the eruption of the minifilament is analogous to ejective eruptions of typical large-scale cases. (Some standard jets appear to be weak versions of such

ejective jets.) The drawings in Fig. 2 are tailored to depict the jet in Fig. 1, jet 18 in Extended Data Table 1, which is a blowout jet.

The external reconnection of the erupting-minifilament field with the open field also adds a new hot layer to the larger bipole (larger red loop in Fig. 2c); this reconnection product from earlier eruption episodes might have created the “initial” large bipole (large black loops of Fig. 2a). Other possibilities for the initial large bipole are that it, along with with the filament-carrying bipole, are two asymmetric lobes of an anemone field region³³. That anemone region could be due to recently-emerged magnetic flux, or it could have formed over time via surface-flux migration and cancelation³⁴.

A schematic for X-ray jets similar to that of our Figure 2 was presented by Shibata (1999)¹¹, in Figure 8b of that paper. That figure was derived from data from earlier satellite missions, prior to the high resolution, high-cadence, multiple-EUV-wavelength data of SDO/AIA. There is however a difference between that picture for jets and our picture. The proposal there¹¹ is that a plasmoid (which might correspond to our minifilament) erupts from the external-reconnection site of the emerging-flux model (Extended Data Fig. 1), the pre-eruption plasmoid being in the current sheet between the emerging flux and the ambient coronal field. (Also, Figure 6 of that same paper¹¹ explicitly depicts an emerging-flux origin for X-ray jets.) In contrast, our proposal is that X-ray jets, at least in coronal holes, are a miniature version of the standard model for large-scale flares and CMEs, independent of whether there is emerging flux. In our view, prior to eruption the minifilament resides in sheared field (or in a flux rope) in the core of a magnetic arcade, instead of in a current sheet. More generally, in our view the triggering and eruption of the minifilament

may include any of a multitude of processes and subprocess proposed for large-scale eruptions, including those listed in the main text, and others^{7,37,38,40}. Determining whether the pre-eruption minifilaments that erupt in jets are located at an external-reconnection current sheet as suggested by Shibata (1999)¹¹, or instead reside in a magnetic arcade as we picture, requires further observational study.

In AIA movies the developing jets show clear rotation in some cases, such as the jet of Figure 1 (Extended Data Video 1def). Other jets however show only partial rotation (e.g., Extended Data Figure 2, and Extended Data Videos 2abc and 2def), or no obvious rotation (e.g., Extended Data Figure 3, and Extended Data Videos 3abc and 3def). Since we have not identified a clear pattern regarding the rotations and the resulting jets, we do not address this topic further here.

Cause of minifilament-eruption onset. Since in this study we do not examine jets that originate at low solar latitudes, we cannot adequately see the causes (triggering) of these magnetic eruptions. As with large-scale filament eruptions, several triggering agents could be responsible, including flux cancelation or even flux emergence. Our main point here is that, independent of the cause of the minifilament-eruption onset, the jets all result from those minifilament eruptions, with the JBP being the “flare” occurring in conjunction with those minifilament eruptions.

As stated in the main text however, several other studies^{13,29,30} found on-disk coronal jets clearly to occur in conjunction with magnetic flux cancelation. One study¹³ aggressively searched for emerging flux beneath a jet, but found no significant signature of emergence. A different study³⁵ also searched for but did not find emerging flux below an on-disk coronal jet. Another

study⁴¹ found mini-CMEs resulting from perhaps “small filament ejections”, that may be similar or identical to the jets we discuss here; they report the ejections to occur at sites of “twisting small concentrations of opposite polarity magnetic field”, and again they do not report detections of emerging flux. Similar jets were reported elsewhere⁴², but without direct magnetic field observations.

We have found two studies of on-disk jets where emerging flux was reported. In the first of these⁴³, although emergence occurred, a microflare and an EUV jet happened only after cancellation of flux in the region of the flux emergence. Similarly, in the second study⁴⁴ flux emergence occurred, but, for two different jets they observed, both jets occurred at about the time the emerged flux underwent cancellation with neighboring field. In that second case, the jet observations were from XRT, and were of jets occurring in on-disk coronal holes; thus those observations are on-disk complementary examples of the near-limb XRT polar-coronal-hole jet observations we present in this paper.

On balance then, the on-disk coronal jet studies suggest that flux cancellation is often crucial to jet onset. In light of the present study, we expect that in those earlier observations, the cancellation likely resulted in minifilament eruptions that produced jets, with flares occurring in the wake of those eruptions and appearing as JBPs.

Additional References (see main text for 1-30)

31. Crooker, N. U., Gosling, J. T. & Kahler, S. W. Reducing heliospheric magnetic flux from coronal mass ejections without disconnection. *J. Geophys. Res.* **107**, 1028–1032 (2002).
32. Moore, R. L., Cirtain, J. W., Sterling, A. C. & Falconer, D. A. Dichotomy of solar coronal jets: Standard jets and blowout jets. *Astrophys. J.* **720**, 757–770 (2010).
33. Shibata, K. *et al.* Chromospheric anemone jets as evidence of ubiquitous reconnection. *Science* **318**, 1591–1594 (2007).
34. Innes, D. & Teriaca, L. Quiet sun explosive events: jets, splashes, and eruptions. *Solar Phys.* **282**, 453–469 (2013).
35. Chandrashekar, K., Morton, R. J., Banerjee, D. & Gupta, G. R. The dynamical behaviour of a jet in an on-disk coronal hole observed with AIA/SDO. *A&A* **562**, A98–A107 (2014).
36. Sterling, A. C., Moore, R. L., & Freeland, S. L. Insights into filament eruption onset from Solar Dynamics Observatory observations. *Astrophys. J.* **731**, L3–L8 (2011).
37. Shibata, K., & Tanuma, S. Plasmoid-induced-reconnection and fractal reconnection. *Earth, Planets and Space* **53**, 473–482 (2001).
38. Lin, J., Forbes, T. G. & Isenberg, P. A. Prominence eruptions and coronal mass ejections triggered by newly emerging flux. *JGR* **106**, 25053–25074 (2001).
39. Chen, P. F. Coronal Mass Ejections: Models and Their Observational Basis. *Liv. Rev. in Solar Phys.* **8**, 1–92 (2001).

40. Kusano, K., Bamba, Y. , Yamamoto, T. T., Iida, Y., Toriumi, S. & Asai, A. Magnetic Field Structures Triggering Solar Flares and Coronal Mass Ejections. *Astrophys. J.* **760**, 31–39 (2012).
41. Innes, D. E., Genetelli, A., Atie, R. & Potts, H. E. Quiet Sun mini-coronal mass ejections activated by supergranular flows. *A&A* **495**, 319–323 (2009).
42. Schrijver, C. J. Eruptions from solar ephemeral regions as an extension of the size distribution of coronal mass ejections. *ApJ* **710**, 1480–1485 (2010).
43. Liu, C., Deng, N., Liu, R. Ugarte-Urra, I., Wang, S.& Wang, H. A standard-to-blowout jet. *ApJ* **735**, L18–L24 (2011).
44. Huang, Z., Madjarska, M. S., Doyle, J. G. & Lamb, D. A. Coronal hole boundaries at small scales iv. SOT view. Magnetic field properties of small-scale transient brightenings in coronal holes. *A&A* **548**, A62–A80 (2012).
45. Pariat, E., Antiochos, S. K., & De Vore, C. R. A model for solar polar jets. *ApJ* **74**, 61–74 (2009).

Extended Data Follow

Extended Data Table 1: X-Ray Jets of This Study

Event	Date ^a	Start; End ^b	x, y (arcsec) ^c	Type ^d	Fil. Size ^e (arcsec)	Fil. Speed ^e (km s ⁻¹)
1	2010 Jul 24	15:56; >16:15	-60, 950	blowout	17	14 ± 2
2	2010 Jul 25	12:29; 12:46	140, -950	blowout	10	30 ± 10
3	2010 Aug 26	14:13; >14:16	100, 950	blowout	10	28 ± 5
4	2010 Jul 27	11:35; 12:17	30, 920	standard	20 ^f	50 ± 5 ^f
5	2010 Jul 27	11:40; 12:20	-50, 920	standard	diffuse(?) ^f	28 ± 5(?) ^f
6	2010 Aug 28	11:40; 12:03	-130, 940	standard	5	28 ± 5
7	2010 Aug 28	<13:41; >13:48	-70, 840	standard	17	rolling
8	2010 Sep 05	21:14; 21:35	30, 840	blowout	10	28 ± 5
9	2010 Sep 08	01:29; 01:44	40, 935	blowout	6	19 ± 5
10	2010 Sep 09	20:14; 20:33	20, 770	blowout	17	73 ± 8
11	2010 Sep 09	20:21; 20:40	60, 850	ambiguous	12	uncertain ^g
12	2010 Sep 09	22:05; 22:31	0, 910	blowout	7	13 ± 3
13	2010 Sep 09	23:52; 00:06	-120, 950	blowout	9	33 ± 5
14	2010 Sep 10	00:01; 00:09	-10, 880	blowout	7	50 ± 10
15	2010 Sep 11	00:39; 00:50	80, 950	blowout	8 ^f	19 ± 5 ^f
16	2010 Sep 11	<01:08; 01:27	-120, 950	blowout	13	40 ± 8
17	2010 Sep 17	20:39; 21:08	-20, 840	blowout	diffuse ^h	33 ± 8 ^h
18	2010 Sep 17	22:08; 22:18	30, 960	blowout	7	40 ± 5
19	2010 Sep 19	19:47; 20:23	20, 880	standard	10	20 ± 5
20	2010 Sep 27	00:39; 00:43	0, 960	blowout	10	20 ± 5

(a) Date of event start time.

(b) UT time period of clearly-detectable jet and/or compact X-ray jet bright point (JBP) in XRT images.

Symbols “<” and “>” respectively indicate the jet started before or continued after indicated times during gaps in XRT data.

(c) Approximate x, y location of jet in AIA images in heliocentric coordinates.

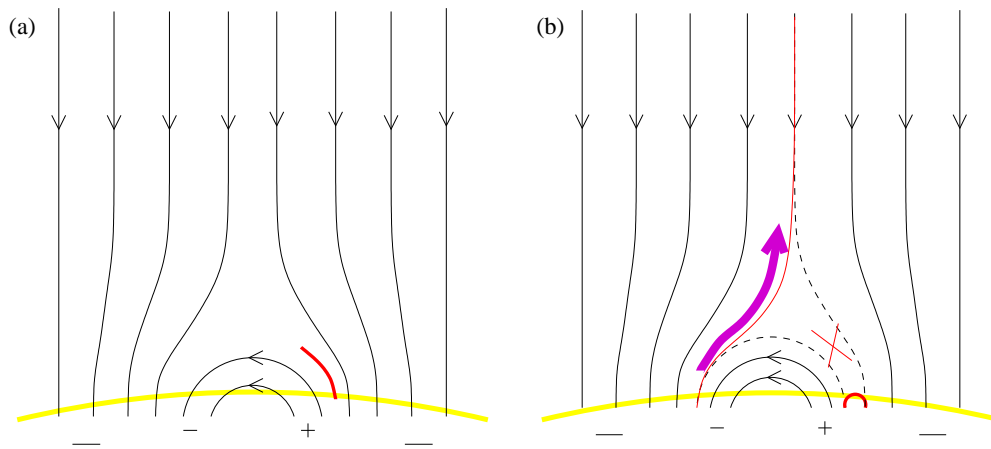
(d) Morphological classification of X-ray jet based on Moore *et al.*¹⁵ study.

(e) Line-of-sight projected size/speed of minifilament near time of eruption onset; size uncertainty $\lesssim 3''$.

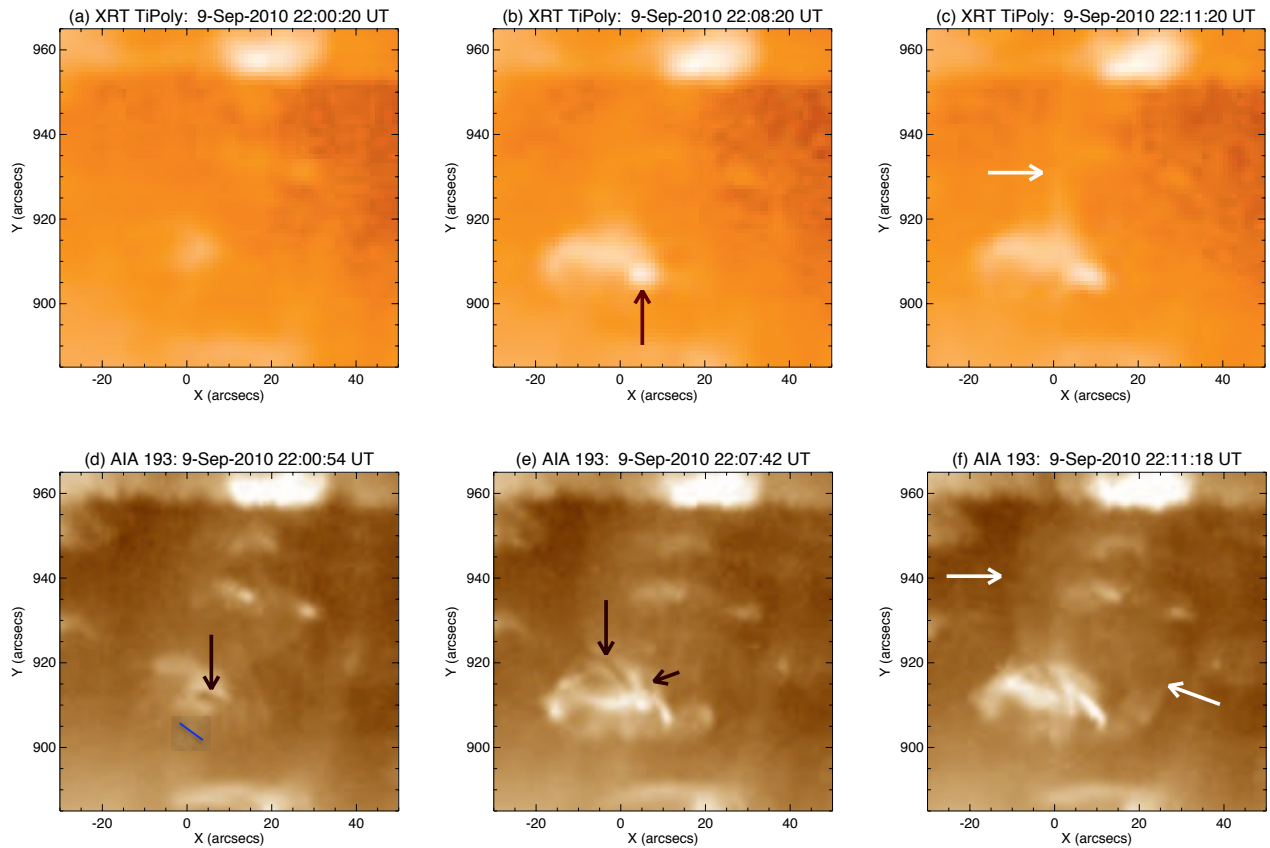
(f) Minifilament diffuse, faint, or identification less certain than other cases.

(g) Accurate speed measurement not possible due to image shifts during eruption time.

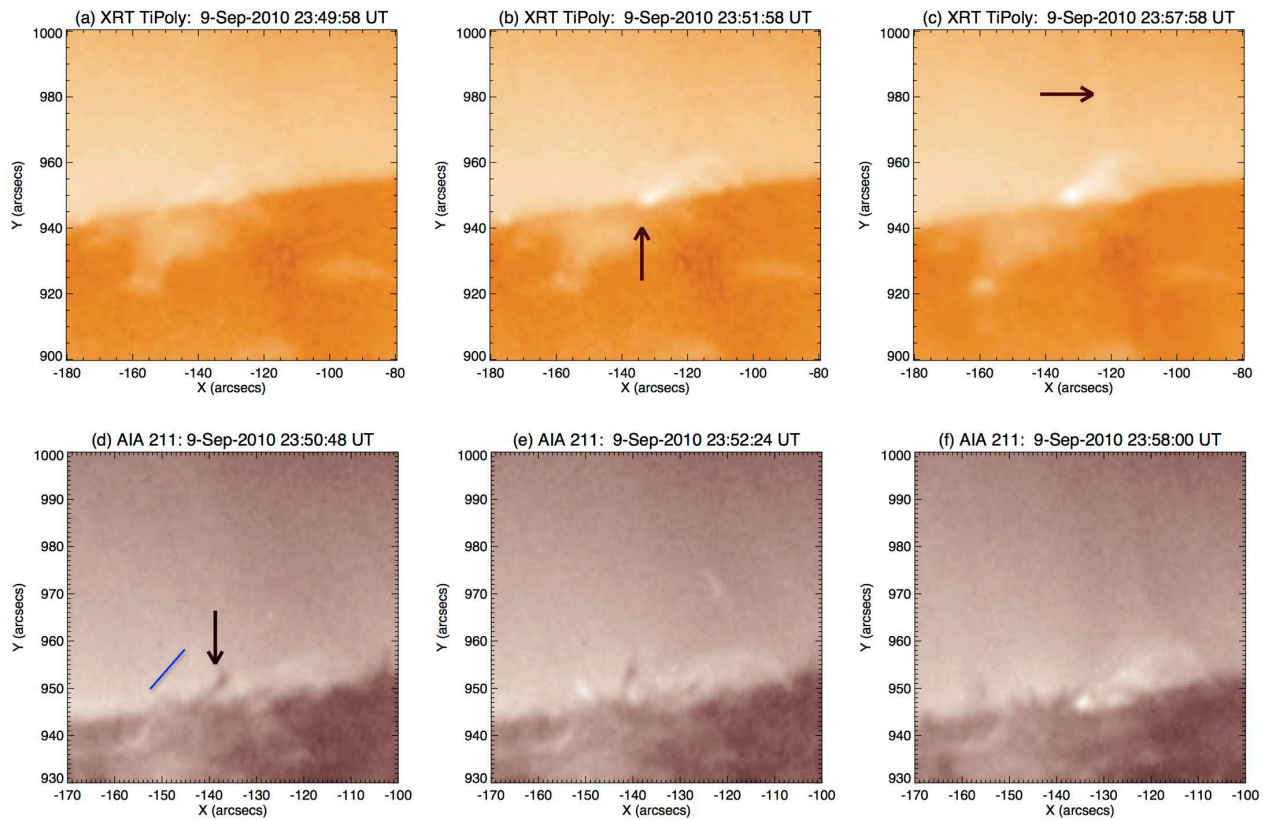
(h) Minifilament too diffuse for size measurement, but moving structures can be tracked for velocity estimate.



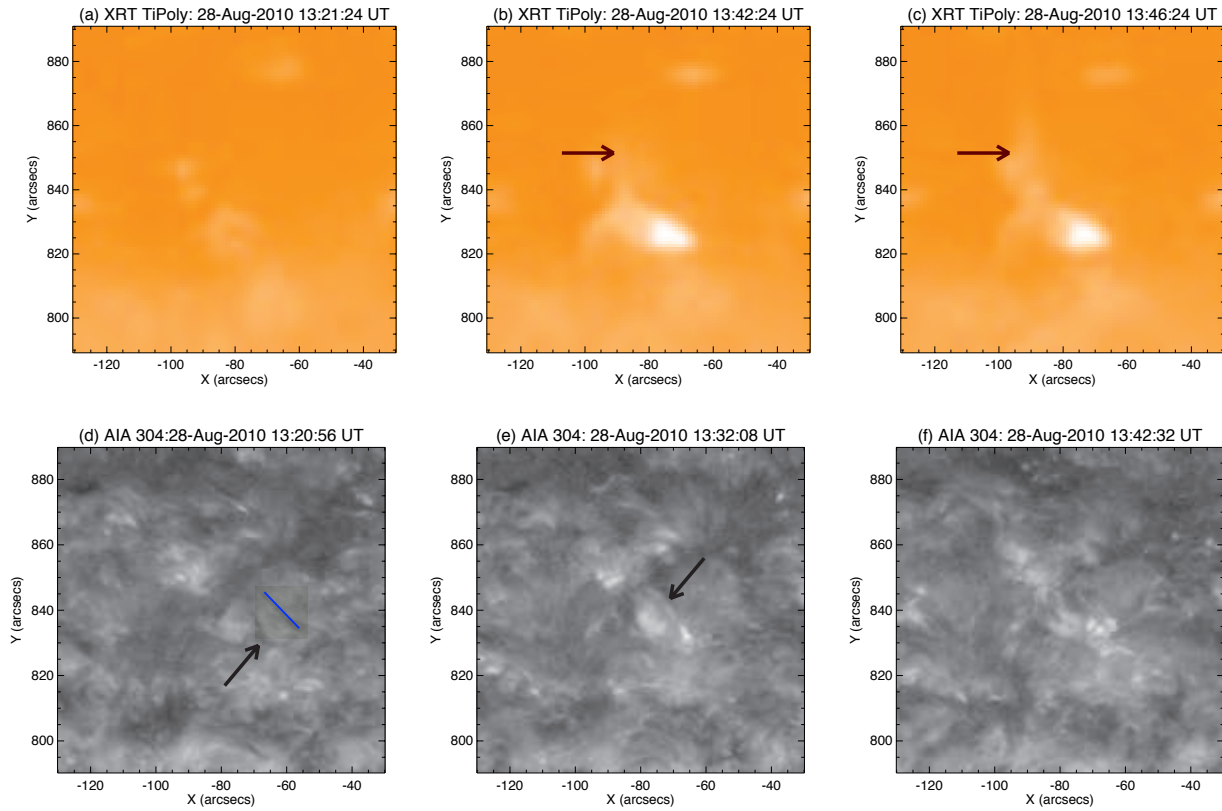
Extended Data Figure 1. Emerging-Flux Model for Solar Jets. Schematic representation of the commonly-accepted solar X-ray-jet-formation mechanism¹. Lines and red cross are as in Fig. 2, and the red curve in (a) represents a current sheet. Flux emergence purportedly forces reconnection at the current sheet (red cross), resulting in new closed loop field (red loop), and new connections to the open coronal field (red curve), along which the X-ray jet (magenta) flows. According to this model, the new reconnection loops appear as the JBP. Previous scenarios for “blowout jets”^{15,32,45} have been variations of this model.



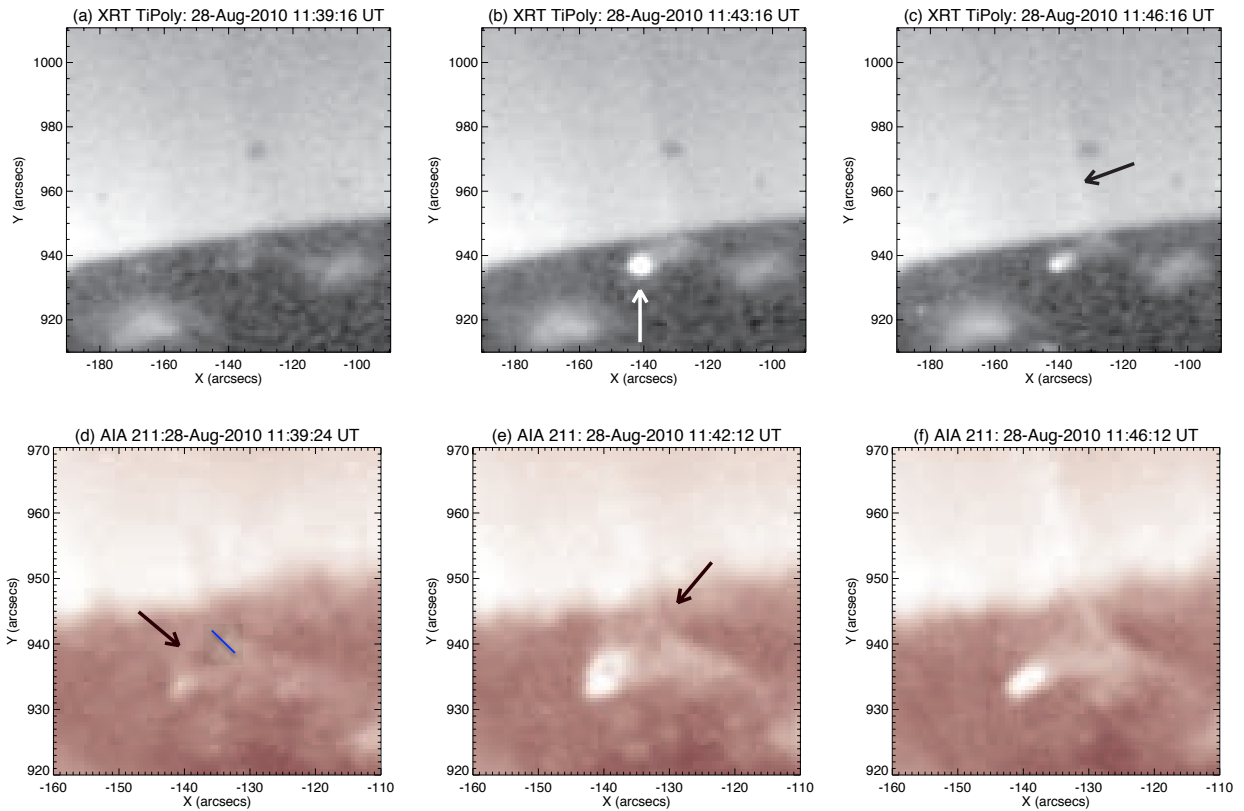
Extended Data Figure 2. Extended Data Table 1 Event 12 Jet. XRT (a—c) and AIA 193Å (d—f) images of the jet. Arrows show: (b) developing JBP; (c) X-ray-jet spire; (d) minifilament; in (e) both arrows point to segments of the minifilament, which split during eruption; (f) both arrows point to edges of a broad jet. In (d) the blue bar shows our estimate of the size of the minifilament, the value of which appears in Extended Data Table 1. See Extended Data Video 2abc and 2def for animations.



Extended Data Figure 3. Extended Data Table 1 Event 13 Jet. XRT (a—c) and AIA 211 Å (d—f) images of the jet. Dark feature in upper-right of XRT images is an artifact. Arrows show: (b) developing JBP; (c) X-ray-jet spire; (d) minifilament starting to erupt. Blue bar in (d) is as in Extended Data Fig. 2. AIA images are zoomed-in more than XRT images. See Extended Data Video 3abc and 3def for animations.



Extended Data Figure 4. Extended Data Table 1 Event 7 Jet. XRT (a—c) and AIA 304Å (d—f) images of a “standard” jet. Arrows show: (b) X-ray jet spire; (c) X-ray jet spire, showing drift since (b); (d) minifilament starting to erupt; (e) “rolling” filament (see Methods). Blue bar in (d) is as in Extended Data Fig. 2. Grey-scale (d—f) shows filament better than colour for this event. See Extended Data Video 4abc and 4def for animations.



Extended Data Figure 5. Extended Data Table 1 Event 6 Jet. XRT (a—c) and AIA 211Å (d—f) images of a “standard” jet. Dark spot north-west of center in XRT images is an artifact. Arrows show: (b) JBP; (c) X-ray jet spire; (d) minifilament moving upward; (e) minifilament near apex of jet base, with jet spire starting to develop. AIA images are zoomed-in more than XRT images. Blue bar in (d) is as in Extended Data Fig. 2. See Extended Data Video 5abc and 5def for animations.